LEVERAGING CHORIONIC VILLUS BIOPSIES FOR THE DERIVATION OF PATIENT-SPECIFIC TROPHOBLAST STEM CELLS

Kaela M. Varberg[1,†,*], Ayelen Moreno-Irusta[1,†], Allynson Novoa[2], Boryana Koseva[3,4], Brynne Musser[1], Joseph M. Varberg[5], Jeremy P. Goering[6], Irfan Saadi[6], Hiroaki Okae[7], Takahiro Arima[7], John Williams III[8,9], Elin Grundberg[1,3,4], Margareta D. Pisarska[2,8,9,10*], and Michael J. Soares[1,4,11,*]

[1]Institute for Reproductive and Developmental Sciences, Department of Pathology & Laboratory Medicine, University of Kansas Medical Center, Kansas City, KS 66160

[2]Division of Reproductive Endocrinology and Infertility, Department of Obstetrics and Gynecology, Cedars-Sinai Medical Center, Los Angeles, CA

[3]Genomic Medicine Center, Children's Mercy Research Institute, Children's Mercy Kansas City, Kansas City, MO

[4]Center for Perinatal Research, Children's Mercy Research Institute, Children's Mercy, Kansas City, MO 64108

[5]Stowers Institute for Medical Research, Kansas City, MO, 64110

[6]Department of Cell Biology and Physiology, University of Kansas Medical Center, Kansas City, KS 66160

[7]Department of Informative Genetics, Environment and Genome Research Center, Tohoku University Graduate School of Medicine, Sendai 980-8575, Japan

[8]Department of Obstetrics and Gynecology, Cedars-Sinai Medical Center, Los Angeles, CA

[9]David Geffen School of Medicine, University of California, Los Angeles, CA

[10]Department of Biomedical Sciences, Cedars-Sinai Medical Center, Los Angeles, CA

[11]Department of Obstetrics and Gynecology, University of Kansas Medical Center, Kansas City, KS 66160

Running title: Chorionic villus-derived human TS cells

[†]Authors contributed equally to the manuscript.

***Correspondence:** Kaela M. Varberg, kvarberg@kumc.edu; Margareta D. Pisarska, margareta.pisarska@cshs.org; Michael J. Soares, msoares@kumc.edu

Keywords: trophoblast stem cells, chorionic villus sampling, placental development

Abstract

Human trophoblast stem (**TS**) cells are an informative in vitro model for the generation and testing of biologically meaningful hypotheses. The goal of this project was to derive patient-specific TS cell lines from clinically available chorionic villus sampling (**CVS**) biopsies. Cell outgrowths were captured from human CVS tissue specimens cultured in modified human TS cell medium. Cell colonies emerged early during the culture and cell lines were established and passaged for several generations. Karyotypes of the newly established CVS-derived trophoblast stem (**TS^{CV}**) cell lines were determined and compared to initial genetic diagnoses from freshly isolated chorionic villi. Phenotypes of TS^{CV} cells in the stem state and following differentiation were compared to cytotrophoblast-derived TS (**TS^{CT}**) cells. TS^{CV} and TS^{CT} cells uniformly exhibited similarities in the stem state and following differentiation into syncytiotrophoblast. These shared features included morphology and gene expression. TS^{CV} cell differentiation into extravillous trophoblast cells exhibited cell line dependent phenotypes. CVS tissue specimens provide a valuable source for TS cell derivation. They expand the genetic diversity of available TS cells and are associated with defined clinical outcomes. TS^{CV} cell lines provide a new set of experimental tools for investigating trophoblast cell lineage development.

Introduction

Chorionic villus sampling (**CVS**) represents a standard, prenatal care procedure that is performed between 10-14 weeks of gestation (Stranc et al., 1997). Sampling involves the removal of a small amount of chorionic villus tissue, for the purpose of genetic testing. Common indications for retrieving chorionic villus tissue include advanced maternal age, history of infertility, family history, including another child with genetic anomalies, or an abnormal noninvasive prenatal test result (Pisarska et al., 2016; Stranc et al., 1997). In addition to their use in genetic diagnosis, first trimester chorionic villus tissue has become a robust platform for investigation of placental pathobiology (Flowers et al., 2021; Gonzalez et al., 2021; Pisarska et al., 2016). Chorionic villi are comprised of several cell types including trophoblast cells, mesenchymal cells, macrophages, and cells comprising fetal blood vessels (Aplin and Jones, 2021; Sun et al., 2020). The villus trophoblast cell compartment includes two primary populations, i) cytotrophoblast and ii) terminally differentiated syncytiotrophoblast (**STB**; Aplin and Jones, 2021). Cytotrophoblast have

the capacity to self-renew, and to differentiate into either extravillous trophoblast (**EVT**) cell or STB lineages (Knöfler et al., 2019; Soares et al., 2018). Regulatory mechanisms underlying human cytotrophoblast self-renewal and differentiation have largely remained elusive.

In 2018, conditions for capturing and maintaining human trophoblast stem (**TS**) cells in vitro were first described (Okae et al., 2018). Human TS cells have the capacity for self-renewal and differentiation into EVT cells or STB. This in vitro model system has led to the generation of new insights into mechanisms regulating human trophoblast cell development (Bhattacharya et al., 2020; Hornbachner et al., 2021; Ishiuchi et al., 2019; Jaju Bhattad et al., 2020; Muto et al., 2021; Perez-Garcia et al., 2021; Ruane et al., 2022; Saha et al., 2020; Shahbazi et al., 2020; Shannon et al., 2022; Sheridan et al., 2021; Takahashi et al., 2019; Varberg et al., 2021). Initial human TS cell lines were derived from blastocysts, or first trimester placental tissue obtained from pregnancy terminations. Establishment of culture conditions for human TS cells led to the derivation of TS cells from pluripotent stem cells (Castel et al., 2020; Cinkornpumin et al., 2020; Dong et al., 2020; Guo et al., 2021; Io et al., 2021; Liu et al., 2020; Wei et al., 2021; Yanagida et al., 2021). In this study, we derived patient-specific human TS cell lines from clinically available CVS tissue. Derivation of TS cell lines from CVS tissue expands the genetic diversity of available human TS cells and importantly is linked to clinical data describing pregnancy outcomes.

Results

Derivation of TS cells from CVS biopsies

CVS biopsies were acquired with patient consent as part of standard medical care. Surplus tissue fragments not used for clinical genetic testing were cultured using modified human TS cell conditions (**Fig. 1A**). Tissue pieces attached to type IV collagen-coated tissue culture treated plates (**Fig. 1B**). Cell outgrowths were evident at sites of attachment and expanded over the first several weeks of culture (**Supplementary Fig 1**). Cells and tissue fragments were passaged prior to reaching confluency and replated in 24 well plates. Cell colonies emerged after first passage and steadily expanded with culture medium changes every two days. Colony morphology and growth rates were heterogeneous for the first few passages but became more homogenous thereafter. The morphology of CVS tissue-derived TS

(**TS^{CV}**) cells was consistent with the morphology of cytotrophoblast-derived TS cells (**TS^{CT}**; **Fig. 1B, 2A**). TS^{CV} cell line expansion was carried out slowly to reduce clonal pressure on derived cells. Cell lines were slowly transitioned into 6 well and 10 cm plate formats after passages 3-4 and 7-8, respectively (**Supplementary Fig. 1**). Newly established cell lines were cryopreserved beginning at passage 6. Importantly, TS^{CV} cells tolerated cryopreservation. Revived cells survived, attached, and proliferated for further expansion. Overall, TS^{CV} cell line derivation required approximately three months from sample acquisition to functional assessments of derived lines.

The success rate of TS^{CV} line derivation was 50%, with five TS^{CV} lines (3 XY; 2 XX) successfully derived from 10 unique patient tissue specimens (6 XY; 4 XX; **Table 1**). Success in cell line derivation may be impacted by the negative consequences of overnight shipping or the cellular contents of the tissue fragments but did not appear to be associated with the clinical karyotype of the CVS specimens. Maternal age range was 31-46 with a mean age of 37.5 years and race was predominantly white/Caucasian and non-Hispanic/Latino ethnicity. Maternal and paternal ancestries were varied (**Table 1**). CVS tissue specimen collection ranged from 10-14 weeks gestation with an average gestational age of 12 weeks, 3 days (87 days; **Table 1**). The earliest sample was collected at 10 weeks, 6 days gestation and the latest sample was collected at 13 weeks, 6 days gestation. The amount of starting tissue ranged from 5-20 mg with a mean of 9.1 mg of tissue (**Table 1**). Clinical genetics performed on tissue specimens at the time of CVS indicated that five samples had normal karyotypes (4 samples 46, XY and 1 sample 46, XX). Clinical karyotyping of the remaining five samples reported genomic abnormalities including two samples with trisomy 18 (47, XX, +18 and 47, XY, +18), one sample with trisomy 21 (47, XX, +21), and two samples with chromosomal translocations (**Table 1**). The five derived TS^{CV} cell lines were from three samples with clinically normal karyotypes (TS^{CVK01}, TS^{CVK05}, and TS^{CVK09}), one with trisomy 21 (TS^{CVK08}) and one with a translocation (TS^{CVK07}). Karyotyping was repeated on TS^{CV} cells following line derivation and expansion. Cell line karyotypes were largely consistent with the clinical karyotyping (**Table 1**). Karyotypes of TS^{CVK01}, TS^{CVK05}, and TS^{CVK08} lines displayed complete consistency with the clinical result. TS^{CVK07} and TS$^{CV\text{-}K09}$ cell lines exhibited mosaicism. The karyotype for TS^{CVK07} reflected the translocation between chromosomes 11 and 22 identified during clinical assessment in addition to other anomalies

reported in a smaller subset of cells. Forty percent of the cells karyotyped for TS^{CVK09} were 46, XY. The remaining 60% of cells analyzed displayed other genetic anomalies, however each individual anomaly was restricted to 1-2 total cells (**Table 1**).

Characterization of TS^{CV} cells in the stem state

TS^{CT27} (XX) and TS^{CT29} (XY) served as reference standard human TS cell lines (Okae et al., 2018) used for comparative characterization of the TS^{CV} cell lines. TS^{CV} cells were maintained in a stem/proliferative state and propagated beyond the Hayflick limit of 50 cell divisions for non-stem cells, which is consistent with TS^{CT} cell proliferation (Okae et al., 2018). All established TS^{CV} cell lines were assessed for presence of mycoplasma by quantitative polymerase chain reaction (**qPCR**) and no evidence of contamination was detected. TS^{CV} cells in the stem state grew in discrete colonies and displayed a cobblestone morphology, consistent with the morphology of cytotrophoblast-derived cell lines, TS^{CT27} and TS^{CT29} (Okae et al., 2018) (**Fig. 2A**). TS^{CV} cells displayed additional characteristics consistent with their trophoblast cell identity (Lee et al., 2016), including expression of microRNAs from the Chromosome 19 microRNA cluster (**Fig. 2B; C19MC**; hsa-miR-517a-3p and hsa-miR-526b-3p) and hypomethylation of the E74 Like ETS Transcription Factor 5 (***ELF5***) promoter relative to induced pluripotent stem (**iPS**) cells (**Fig. 2C**). Overall, TS^{CV} and TS^{CT} cells cultured in the stem state displayed similar proliferative, morphologic, microRNA expression, and methylation properties.

Analysis of the differentiation capacity of TS^{CV} cells

Comparisons of TS^{CV} and TS^{CT} cell capacities for differentiation into STB and EVT cell lineages, were performed following cell line derivation (**Supplementary Fig. 1**). Assessments of cell differentiation were routinely performed following 10 passages. Differentiation was assessed at morphological and functional levels.

STB differentiation. The ability of TS^{CV} cells to differentiate into STB was assessed using the previously described three-dimensional STB (**ST3D**) protocol (Okae et al., 2018). STB differentiation elicited significant morphological changes, including the formation of suspended spheroid cell clusters

(**Fig. 3A**). Complementary to the morphological changes observed, TS^{CV}-derived STB displayed downregulation of stem state transcripts ***TEAD4***, ***LRP2***, and ***LIN28A*** (**Fig. 3B**) and upregulation of STB lineage-specific transcripts, including cytochrome P450 Family 11 Subfamily 1 (***CYP11A1***), chorionic gonadotropin beta 7 (***CGB7***), and syndecan 1 (***SDC1***; **Fig. 3C**). Overall, all TS^{CV}-derived STB showed similar morphological and expression patterns of signature STB transcripts observed in TS^{CT}-derived STB. STB cell differentiation was also attainable in both TS^{CV} lines possessing abnormal karyotypes. Cyst-like STB morphology was evident in TS^{CVK07} cells (**Supplementary Fig. 2A**) and TS^{CVK08} cells (**Supplementary Fig. 2B**). *CYP11A1*, *CGB7*, and *SDC1* were upregulated in TS^{CVK07} STB and TS^{CVK08} STB compared to the stem state (**Supplementary Fig. 2C, 2D**).

EVT cell differentiation. Canonical features of EVT cell differentiation observed in TS^{CT} cells were evident in a subset of TS^{CV} cell lines possessing a normal karyotype (TS^{CVK01} and TS^{CVK09}), including elongated cell morphology (**Fig. 4A; Videos 1-3**) and expression of major histocompatibility complex, class I, G (**HLA-G**) protein (**Fig. 4B**). EVT cells displayed downregulation of stem state transcripts ***TEAD4***, ***LRP2***, and ***LIN28A*** (**Fig. 4C**). Characteristic EVT transcripts were upregulated, including *HLA-G*, matrix metallopeptidase 2 (***MMP2***), and C-C motif chemokine receptor 1 (***CCR1***; **Fig. 4D**). Overall, these TS^{CV} stem cell derived EVT cells were comparable to EVT cells derived from TS^{CT} cells. TS^{CVK08}, possessing trisomy 21, was also capable of EVT cell differentiation (**Supplementary Fig. 3A-C**). Optimal EVT cell differentiation was not attainable in TS^{CVK05} cells (**Supplementary Fig. 4A-C**), which possesses a normal karyotype, and TS^{CVK07} cells, which possesses an abnormal karyotype (**Supplementary Fig. 4D-F**). Variability in the capacity for human TS cell line differentiation into EVT cells has been previously reported (Cinkornpumin et al., 2020; Haider et al., 2022; Okae et al., 2018; Shannon et al., 2022).

Transcriptomic analysis of the developmental potential of TS^{CV} cells

To obtain a broad and unbiased comparative assessment of TS^{CV} and TS^{CT} in stem, STB, and EVT differentiated cell states, transcriptomes were captured using RNA-sequencing (**RNA-seq**). Principal component analysis of all TS^{CT} and TS^{CV} cell lines identified three primary cell-state specific clusters (**Fig.**

5A). Two outliers that did not cluster within a specific cell state were TS^{CVK05} and TS^{CVK07} cells cultured to promote EVT cell differentiation. Correlation analyses performed to compare cell expression profiles identified comparable transcriptomic changes across TS^{CV} and TS^{CT} cell lines (**Fig. 5B**).

STB differentiation from the stem state resulted in broad changes in gene expression in TS^{CT} cells (**Fig. 5C; Supplementary Table 1**) and TS^{CV} cells (**Fig. 5D; Supplementary Table 2**), including downregulation of stem markers *EPCAM, LIN28A, LRP2, PEG10, and TEAD4* and upregulation of STB markers *CGB2, CGB7, CYP11A1*, *CYP19A1,* and *SDC1*. STB differentiation-induced changes in gene expression were consistent between TS^{CT} (TS^{CT27} and TS^{CT29}) and TS^{CV} (TS^{CVK01}, TS^{CVK05}, TS^{CVK09}) cells (R=0.88, p<2.23-16; **Fig. 5E**). TS cells possessing abnormal karyotypes also displayed consistent clustering for the STB lineage (**Fig. 5A**, **5B**). STB gene expression profiles were evident in TS^{CVK07} (**Supplementary Fig. 5A Supplementary Table 3**) and TS^{CVK08} (**Supplementary Fig. 5B**; **Supplementary Table 4**) cells. The STB profiles were consistent with gene expression changes observed in TS^{CT} cells as evidenced by strong correlations with TS^{CVK07} (R=0.83, p<2.23-16; **Supplementary Fig. 5C**) and TS^{CVK08} (R=0.84, p<2.23-16; **Supplementary Fig. 5D**) cells. Overall, independent of karyotype, all TS^{CT} and TS^{CV} lines could undergo successful STB differentiation.

TS^{CVK01}, TS^{CVK08}, TS^{CVK09} cells induced to differentiate into EVT cells clustered with EVT cells differentiated from TS^{CT} cell lines (**Fig. 5A**). In contrast, transcriptomes for TS^{CVK05} and TS^{CVK07} cells cultured in conditions promoting EVT cell differentiation clustered independent of stem state, STB and EVT cell clusters (**Fig. 5A**). EVT cells successfully differentiated from the stem state exhibited broad gene expression changes in TS^{CT} (**Fig. 5F; Supplementary Table 5**) and most TS^{CV} cell lines with normal karyotypes (TS^{CVK01} and TS^{CVK09}; **Fig. 5G; Supplementary Table 6**). These changes included the downregulation of stem markers *EPCAM, LIN28A, LRP2, PEG10, and TEAD4* and upregulation of EVT cell markers *CCR1, HLA-G, ITGA1*, *MMP2,* and *NOTUM*. EVT differentiation-induced changes in gene expression were consistent between TS^{CT} (TS^{CT27} and TS^{CT29}) and TS^{CV} (TS^{CVK01} and TS^{CVK09}) cells (R=0.83, p<2.23-16; **Fig. 5H**) as well as between TS^{CT} and TS^{CVK08} cells (R=0.78, p<2.23-16; **Supplementary Fig. 6A, B, Supplementary Table 7**), which possess Trisomy 21. EVT cell differentiation

was less complete in TS^{CVK05} cells (R=0.68, p<2.23-16; **Supplementary Fig. 6C, D**; **Supplementary Table 8**) and in TS^{CVK07} cells (R=0.66, p<2.23-16; **Supplementary Fig. 6E, F**; **Supplementary Table 9**).

In summary, these results indicate that TS^{CV} cells are capable of self-renewal and effective differentiation into both STB and EVT cell lineages and can be considered bonafide TS cells. Differences were noted in the capacity of some TS^{CV} lines for EVT cell differentiation.

Discussion

Our understanding of placenta development and function has benefitted from the availability of in vitro model systems. In the human, these model systems have included primary cell and explant cultures, choriocarcinoma-derived cell lines, and immortalized cell lines (Ringler and Strauss, 1990; Shibata et al., 2020). Each in vitro approach has had merits but also limitations (Lee et al., 2016; Soares et al., 2018). About two decades ago, Rossant and colleagues reported a procedure for culturing TS cells from the mouse (Tanaka et al., 1998). These cells could be maintained in a proliferative stem state or induced to differentiate. Furthermore TS cells could be reintroduced into blastocysts and shown to possess the capacity to contribute to mouse placentas (Tanaka et al., 1998). Mouse TS cells became an effective model system to elucidate gene regulatory networks controlling trophoblast cell differentiation and placental development (Hada et al., 2022; Hemberger et al., 2020; Latos and Hemberger, 2016; Lee et al., 2019). Efforts ensued to establish TS cells in other species with some success (Asanoma et al., 2011; Grigor'eva et al., 2009) but human TS cells represented an enigma (Kunath et al., 2014; Shibata et al., 2020). Culture protocols for sustaining mouse TS cells were ineffective in the human (Kunath et al., 2014). The discovery of culture conditions for propagating and differentiating human TS cells represented a major advancement (Okae et al., 2018). Utilizing these human TS cell culture tools, we have demonstrated the feasibility of capturing and expanding authentic TS cells from human CVS tissue specimens.

The initial human TS cell lines were derived from either blastocysts or first trimester pregnancy terminations (Okae et al., 2018). These human TS cell lines represent the benchmark for all TS cell lines subsequently derived. CVS biopsies are an alternative tissue source for deriving TS cells. They are

retrieved during the first trimester of pregnancy as part of standard medical care (Adusumalli et al., 2007; Dong et al., 2003; McIntosh et al., 1993; Pisarska et al., 2016; Stranc et al., 1997; Wang et al., 1994; Williams et al., 1992, 1987). Thus, CVS-derived TS cell lines can be connected to robust pregnancy outcome information. Human TS cell lines have also been successfully derived from pluripotent stem cells (Castel et al., 2020; Cinkornpumin et al., 2020; Dong et al., 2020; Guo et al., 2021; Io et al., 2021; Jang et al., 2022; Liu et al., 2020; Soncin et al., 2022; Viukov et al., 2022; Wei et al., 2021; Yanagida et al., 2021), miscarriages (Saha et al., 2020), and most recently from term human placenta (Wang et al., 2022). These alternative TS cell models are potentially useful tools for investigating trophoblast cell development but each offer caveats for consideration. Pluripotency is established through extensive genomic reprogramming (Hanna et al., 2010; Papp and Plath, 2013), which minimizes the impact of the epigenetic landscape established during pregnancy on the TS cell phenotype. TS cells derived from trophoblast tissue obtained from miscarriages may best contribute to understanding trophoblast cell-related mechanisms linked to pregnancy failure and the impact of a failed pregnancy on TS cells. TS cells recovered from term placental tissue reflect the culmination of events transpiring throughout the duration of pregnancy. It is reasonable to assume that genetic background and source of trophoblast tissue for TS derivation will influence TS cell behavior. Culturing TS cells under optimized conditions may normalize some features attributed to an adverse pregnancy and maternal environment, whereas in other cases the aberrant behavior may persist. Advantages of using CVS-derived TS cells for investigating trophoblast cell-gene regulatory networks contributing to placental development are evident.

TS cell lines were successfully derived from CVS biopsies possessing both normal and abnormal karyotypes. These TS cell lines could be interrogated in the stem state and following differentiation into either STB or EVT. TS cells with a triploid karyotype have also been established from human blastocysts (Kong et al., 2022). Most recently, trophoblast organoids with abnormal karyotypes have been derived from CVS biopsies (Schaffers et al., 2022). The true impact of the chromosomal abnormalities on TS cells and their differentiation into STB or EVT cells will require successful cultivation and characterization of multiple cell lines possessing the same abnormal karyotype.

Mosaicism is a characteristic feature of the human placenta (Coorens et al., 2021; Robinson and Del Gobbo, 2021; Yuen and Robinson, 2011). Trophoblast cells possess a tolerance for karyotypic abnormalities not evident in the embryo or fetus (Coorens et al., 2021; Shahbazi et al., 2020; Yuen and Robinson, 2011). Each cotyledon of the placenta exhibits elements of trophoblast cell clonality (Coorens et al., 2021). Placental mosaicism is manifested in genetic and functional differences among cotyledons within a human placenta (Coorens et al., 2021; Huang et al., 2009; Rubin et al., 1993; Wang et al., 1993). Among the TS cell lines derived from CVS biopsies, some exhibited a karyotype consistent with the karyotype of chorionic villus tissue used for the clinical genetic analysis, whereas others differed. These tissue biopsies contained a mixture of trophoblast and extraembryonic mesoderm contributions (Aplin and Jones, 2021). Thus, differences in TS cell versus chorionic villus tissue could be attributed to confined placental mosaicism or alternatively, linked to an unappreciated consequence of culture conditions required to establish the TS cell lines.

In summary, the generation of CVS-derived human TS cell lines expands the genetic diversity of existing TS cell lines available for basic research, provides an opportunity to associate pregnancy outcomes with trophoblast function, and will provide insight into the importance of genetic anomalies and mosaicism in trophoblast cell development.

Materials and Methods

Chorionic villus tissue collections, karyotypic analysis, and clinical phenotyping

Chorionic villus tissue was obtained by highly experienced perinatologists as part of standard medical care between 10-14 weeks of gestation for clinical genetic diagnosis at Cedars-Sinai Medical Center (Huang et al., 2009; Pisarska et al., 2016). Clinical cytogenetic analysis was performed on tissue specimens by direct and long-term culture and reviewed by a team of cytogeneticists (Huang et al., 2009). Residual trophoblast tissue fragments not required for clinical cytogenetic analysis were recovered, suspended in Complete TS Cell Medium [DMEM/F12 (11320033, Thermo Fisher Scientific), 100 μM 2-mercaptoethanol, 0.2% (vol/vol) fetal bovine serum (**FBS**), 50 μM penicillin, 50 U/mL streptomycin, 0.3% bovine serum albumin (**BSA**, BP9704100, Thermo Fisher Scientific), 1% Insulin-Transferrin-Selenium-Ethanolamine (**ITS-X**) solution (vol/vol, 51500056, Thermo Fisher Scientific)], 8.5 μM L-ascorbic acid (A8960, Sigma-Aldrich), 50 ng/mL epidermal growth factor (**EGF**, E9644, Sigma-Aldrich), 2 μM CHIR99021 (04-0004, Reprocell), 0.5 μM A83-01 (04-0014, Reprocell), 1 μM SB431542 (04-0010, Reprocell), 800 μM valproic acid (P4543, Sigma-Aldrich), and 5 μM Y27632 (04-0012-02, Reprocell)] (Okae et al., 2018), shipped overnight to the University of Kansas Medical Center, and used for TS cell derivation. Demographic data was collected from patients and included, parental ages, races and ethnicities, and ancestry (**Table 1**). All human tissue specimens used for research purposes were collected following informed written consent, deidentified, and approved by institutional review boards at both Cedars-Sinai Medical Center and at the University of Kansas Medical Center.

Derivation of TS cells from CVS tissue specimens

Chorionic villus tissue specimens were placed in 24 well tissue culture-treated dishes coated with 5 mg/mL Corning® mouse type IV collagen (35623, Discovery Labware Inc.) diluted in phosphate buffered saline (**PBS**). Tissue specimen fragments (3-6 pieces per well) were cultured in 300 μL of Complete TS Cell Medium. Tissue fragments attached within 2-5 days. Medium was replaced with fresh TS cell culture medium after initial attachment and every two days thereafter. Time to first passage was unique to each sample and determined by the extent of the outgrowth, but commonly occurred around 21 days post plating. Cells and attached tissue fragments were washed with PBS and detached with TrypLE

Express (12604021, Thermo Fisher Scientific). Cell and tissue fragments were replated in human TS cell culture conditions in a 24 well plate format. Colonies emerged after the first passage. Cells were maintained in 24 well plate format for 3-5 passages and then expanded into 6 well plate format.

TS cell culture

Following TS cell derivation, TS cells were cultured in dishes pre-coated with iMatrix511 (1:2000 dilution; NP892-01, Reprocell). TS cells were maintained in a modified Complete TS Cell Medium [DMEM/F12 (11320033, Thermo Fisher Scientific), 50 μM penicillin, 50 U/mL streptomycin, 0.15% BSA (BP9704100, Thermo Fisher Scientific), 1% ITS-X solution (vol/vol; 51500056, Thermo Fisher Scientific)], 200 μM L-ascorbic acid (A8960, Sigma-Aldrich), 1% KSR (10828028, Thermo Fisher Scientific), 25 ng/mL EGF (E9644, Sigma-Aldrich), 2 μM CHIR99021 (04-0004, Reprocell), 5 μM A83-01 (04-0014, Reprocell), 800 μM valproic acid (P4543, Sigma-Aldrich), and 2.5 μM Y27632 (04-0012-02, Reprocell)] (Takahashi et al., 2019). Cell medium was replaced every two days of culture.

STB differentiation

To induce STB cell differentiation, TS cells were plated into 6 cm petri dishes at a density of 300,000 cells per dish and cultured in ST3D Medium [DMEM/F12 (11320033, Thermo Fisher Scientific), 50 μM penicillin, 50 U/mL streptomycin, 0.15% BSA (BP9704100, Thermo Fisher Scientific), 1% ITS-X solution (vol/vol; 51500056, Thermo-Fisher)], 200 μM L-ascorbic acid (A8960, Sigma-Aldrich), 5% KSR (10828028, Thermo Fisher Scientific), 2.5 μM Y27632 (04-0012, Reprocell), 2 μM forskolin (F6886, Sigma), and 50 ng/mL of EGF (E9644, Sigma)] (Okae et al., 2018). On day 3 of cell differentiation, 3 mL of fresh ST3D medium was added to the culture dishes. Cells were analyzed on day 6 of STB cell differentiation.

EVT cell differentiation

EVT cell differentiation was induced by plating human TS cells onto 6-well plates pre-coated with 1 μg/mL of mouse type IV collagen at a density of 80,000 cells per well. Cells were cultured in EVT Differentiation Medium [DMEM/F12 (11320033, Thermo Fisher Scientific), 100 μm 2-mercaptoethanol,

0.2% (vol/vol) FBS, 50 µM penicillin, 50 U/mL streptomycin, 0.3% bovine serum albumin (BP9704100, Thermo Fisher Scientific), 1% Insulin-Transferrin-Selenium-Ethanolamine solution (vol/vol; 51500056, Thermo Fisher Scientific)], 100 ng/mL of neuregulin 1 (**NRG1**, 5218SC, Cell Signaling, Danvers, MA), 7.5 µM A83-01 (04-0014, Reprocell, Beltsville, MD), 2.5 µM Y27632 (04-0012, Reprocell), 4% KnockOut Serum Replacement (**KSR**, 10828028, Thermo Fisher Scientific), and 2% Matrigel® (CB-40234, Thermo Fisher Scientific). On day 3 of EVT cell differentiation, the medium was replaced with EVT Differentiation Medium excluding NRG1 and with a reduced Matrigel® concentration of 0.5%. On day 6 of EVT cell differentiation, the medium was replaced with EVT Differentiation Medium with a Matrigel concentration of 0.5% and excluding NRG1 and KSR. Cells were analyzed on day 8 of EVT cell differentiation.

Cell line karyotyping

Chromosome analysis of TS^{CV} cells was performed using standard cytogenetic methods (Huang et al., 2009; Pisarska et al., 2016). GTG banded chromosomes were analyzed at 450-550 band levels. Cytogenetic and FISH results were described according to the current International Standing Committee on Human Cytogenetic Nomenclature (International Standing Committee on Human Cytogenetic Nomenclature et al., 2009).

Immunocytochemical analysis

Cells were fixed with 4% paraformaldehyde (Sigma-Aldrich) for 15 min at room temperature. Fixed cells were incubated with primary antibody against HLA-G (ab52455, Abcam), followed by Alexa488-conjugated goat-anti-mouse immunoglobulin G (**IgG**; A32723, Thermo Fisher Scientific) secondary antibody and 4′,6-diamidino-2-phenylindole (**DAPI**; Molecular Probes). Fluorescence images were captured on a Nikon 80i upright microscope (Nikon) with a Photometrics CoolSNAP-ES monochrome camera (Roper).

Pluripotent stem cell culture

Human induced pluripotent stem (**iPS**) cells were cultured in tissue culture plates pre-coated with Matrigel (1:100 dilution; 356231, Corning). iPS cells were maintained in complete iPS Cell Medium

[mTeSR1 Basal Medium + mTeSR1 5X Supplement (85850, STEMCELL) and 10 µM Y27632 (04-0012-02, Reprocell)] and incubated at 37°C and 5% CO_2. After the first day of culture, cells were cultured in complete iPS cell medium without Y27632. Medium was replaced every other day of culture. Cells were passaged or harvested at 80% confluency.

miRNA isolation, cDNA preparation, and quantitative real-time PCR

Total RNA was isolated using mirVana kit (AM1560, Thermo Fisher Scientific), and RNA concentration was measured with the Qubit™ RNA BR Assay Kit (Thermo Fisher Scientific). cDNA synthesis was performed with TaqMan® Advanced miRNA cDNA Synthesis kit (A28007, Thermo Fisher Scientific). RT-qPCR was performed using TaqMan™Fast Advanced Master Mix (4444556, Thermo Fisher Scientific) and targeted miRNAs MIR517a-3p, MIR-526b-3p, and housekeeping miRNA MIR103a-3p (479485_mir, 478996_mir, and 478253_mir; TaqMan™ Advanced miRNA Assays, Thermo Fisher Scientific; **Supplementary Table 10**). Relative expression of each transcript was calculated using ΔΔCT method and normalized to hsa-miR-103a-3p.

Methylation Analysis

Genomic DNA was isolated using the DNeasy Blood and Tissue Kit (69504, Qiagen), and 500 ng of DNA was bisulfite converted using the EZ DNA Methylation-Gold Kit (D5005, Zymo Research) according to instructions. Following bisulfite conversion, the ELF5 promoter region was amplified using a nested PCR approach with previously reported primers (Primer Set A: forward: 5'-GGAAATGATGGATATTGAATTTGA-3'; reverse: 5'-CAATAAAAATAAAAACACCTATAACC-3' Primer Set B: forward: 5'-GAGGTTTTAATATTGGGTTTATAATG-3'; reverse: 5'-ATAAATAACACCTACAAACAAATCC-3'; **Supplementary Table 11; Lee et al., 2016; Soncin et al., 2022)**. PCR was performed with a hot start DNA polymerase, ZymoTaq (E2001, Zymo Research). After the second PCR, Taq polymerase-amplified PCR products were gel-purified with QIAquick Gel Extraction Kit (28706X4, Qiagen), using manufacturer protocols. The purified DNA was inserted directly into a plasmid vector using TOPO® TA Cloning® Kits for Sequencing (450030, Thermo Fisher Scientific) according to manufacturer instructions. One microliter of purified PCR product was cloned into the

plasmid vector (pCR™4-TOPO®) for 5 min at room temperature. Competent *E. coli* were transformed with the pCR4-TOPO construct, cultured, and minipreps were prepared using the QIAprep Spin Miniprep Kit (27106X4, Qiagen). Purified DNA was sequenced (Genewiz).

RNA isolation and RT-qPCR

Total RNA was isolated using TRIzol®/chloroform precipitation (15596018, Thermo Fisher Scientific) as previously reported (Varberg et al., 2021). cDNA was synthesized from 1 μg of total RNA using the High-Capacity cDNA Reverse Transcription Kit (4368813, Thermo Fisher Scientific) and diluted 10 times with ultra-pure distilled water. qPCR was performed using PowerSYBR® Green PCR Master Mix (4367659, Thermo Fisher Scientific) and primers (250 nM each). RT-qPCR primer sequences are presented in **Supplementary Table 12**. Amplification and fluorescence detection were measured with a QuantStudio 5 Flex Real-Time PCR System (Thermo Fisher Scientific). An initial step (95°C, 10 min) preceded 40 cycles of a two-step PCR (92°C, 15 s; 60°C, 1 min) and was followed by a dissociation step (95°C, 15 s; 60°C, 15 s; 95°C 15 s). The comparative cycle threshold method was used for relative quantification of the amount of mRNA for each sample normalized to the housekeeping genes *B2M* or *POLR2A*.

RNA library preparation and RNA-Seq

Stranded mRNA-sequencing was performed on the Illumina NovaSeq 6000 Sequencing System in the Genomics Core at the University of Kansas Medical Center. Quality control was completed with the RNA Screen Tape Assay kit (5067-5576, Agilent Technologies) on the Agilent TapeStation 4200. Total RNA (1 μg) was processed in the following steps: i) oligo dT bead capture of mRNA, ii) fragmentation, iii) reverse transcription, iv) cDNA end repair, v) Unique Dual Index (**UDI**) adaptor ligation, vi) strand selection, and vii) library amplification using the Universal Plus mRNA-Seq with NuQuant library preparation kit (0520-A01, Tecan Genomics). Library validation was performed with the D1000 Screen Tape Assay kit (5067-5582, Agilent) on the Agilent Tape Station 4200. Library concentrations were determined with the NuQuant module using a Qubit 4 Fluorometer (Thermo Fisher Scientific). Libraries were pooled based on equal

molar amounts and the multiplexed pool was quantified, in triplicate, using the Roche Lightcycler96 with FastStart Essential DNA Green Master (06402712001, Roche) and KAPA Library Quant (Illumina) DNA Standards 1-6 (KK4903, KAPA Biosystems). Using the qPCR results, the RNA-Seq library pool was adjusted to 2.125 nM for multiplexed sequencing. Pooled libraries were denatured with 0.2 N NaOH (0.04N final concentration), neutralized with 400 mM Tris-HCl, pH 8.0, and diluted to 425 pM. Onboard clonal clustering of the patterned flow cell was performed using the NovaSeq 6000 S1 Reagent Kit (200 cycle, 20012864, Illumina). A 2x101 cycle sequencing profile with dual index reads was completed using the following sequence profile: Read 1 – 101 cycles x Index Read 1 – 8 cycles x Index Read 2 – 8 cycles x Read 2 – 101 cycles. Sequence data were converted from .bcl to FASTQ file format using bcl2fastq software and de-multiplexed. Raw FASTQ files were trimmed using default parameters (-r 0.1 -d 0.03) in Skewer (Version 0.2.2) and reads shorter than 18 bp were discarded. Transcripts were quantified using Kallisto (Version 0.46.2). Differentially expressed genes (FDR of 0.05) were discovered using the Bioconductor package DESeq2 in R (Version 1.32.0).

Live cell imaging

Cells were placed into an EVOS Onstage Incubator attached to an EVOS FL Automated Imaging System (Thermo Fisher Scientific). The live cell chamber was maintained at constant temperature (37°C), humidity, and 5% CO_2. For stem culture, TS cells were maintained in stem state culture conditions described above and images were acquired 1-2 days after passage and immediately following culture medium change. EVT cell differentiation was induced as described above. On the fourth day of the EVT cell differentiation protocol, cells were placed into the live cell chamber. Phase contrast images were acquired every 10 min continuously from days 2-4 of stem cell growth or day 4-6 of EVT cell differentiation.

Mycoplasma testing

Mycoplasma presence was assessed using the LookOut® Mycoplasma qPCR Detection Kit (MP0040A, Sigma-Aldrich). Kit protocols were followed as described.

457

458 **Statistical analysis**

459 Statistical analysis was completed with the GraphPad Prism 9 software. Welch's *t* tests, Brown-
460 Forsythe and Welch ANOVA tests were applied when appropriate. The figures depict the data
461 represented as mean ± standard deviation with a statistical significance level of $p<0.05$.

462

463 **Acknowledgements**

464 We thank Stacy Oxley and Brandi Miller for their assistance.

465

466 **Author contributions**

467 K.M.V., M.D.P, and M.J.S. conceived and designed the research; A.N., J.W., and M.D.P. collected and
468 obtained tissue specimens. J.G., I.S., H.O., and T.A. provided reagents, protocols, or equipment; K.M.V.,
469 A.M., B.K., and B.M., performed experiments and/or analyzed data; K.M.V, A.M., J.G, I.S., E.G., M.D.P,
470 and M.J.S. interpreted results of experiments; K.M.V., A.M., J.M.V., and M.J.S. prepared figures and
471 drafted manuscript; K.M.V. M.D.P, and M.J.S. edited and revised manuscript; All authors approved final
472 version of manuscript.

473

474 **Ethics**

475 There is no conflict of interest that could be perceived as prejudicing the impartiality of the research
476 reported.

477

478 **Data availability**

479 All raw and processed sequencing data generated in this study have been submitted to the NCBI Gene
480 Expression Omnibus (GEO; () under accession number GSE #).

Tables and Figures

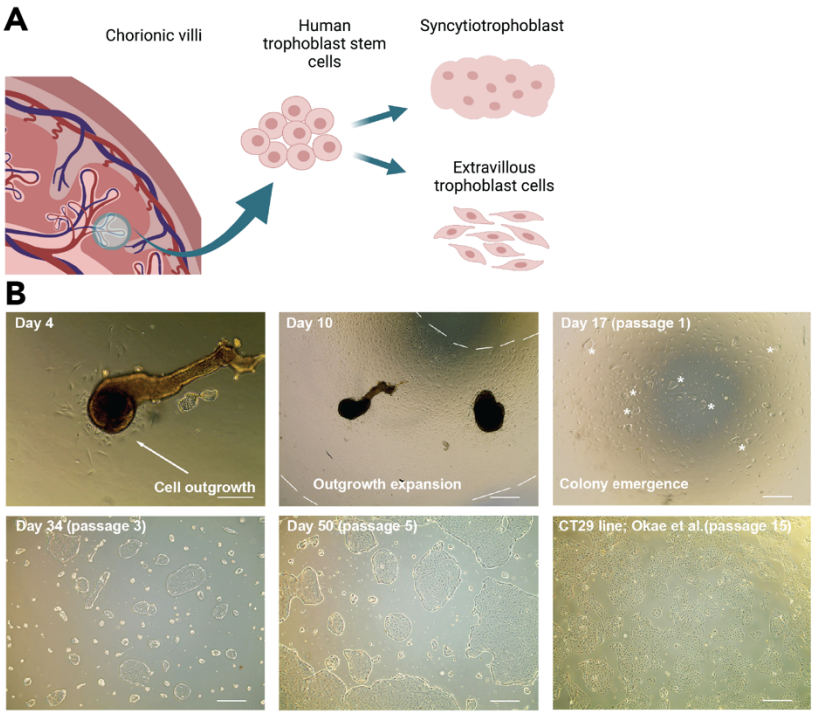

Fig. 1 Deriving TS cells from CVS tissue specimens. A) Simplified schematic depicting the process of obtaining chorionic villi tissue fragments, derivation of TS cells, and then subsequent differentiation into STB and EVT cell lineages. Created with BioRender.com. **B)** Chorionic villus tissue fragments attach and form cellular outgrowths within a few days of initial plating. Within one to two weeks the outgrowths expand and proliferate across the well. Two to three weeks after plating, the cells were passaged, and colonies emerged. Colony clusters were initially small but proliferated and grew rapidly. Significant heterogeneity is present initially, but subsequent passaging selects for a TS cell population that displays a similar morphology to the original TS cell lines (Okae et al., 2018), which possess the ability to differentiate into STB and EVT cell lineages. Scale bar represents 250 μm in first panel. All other scale bars represent 500 μm.

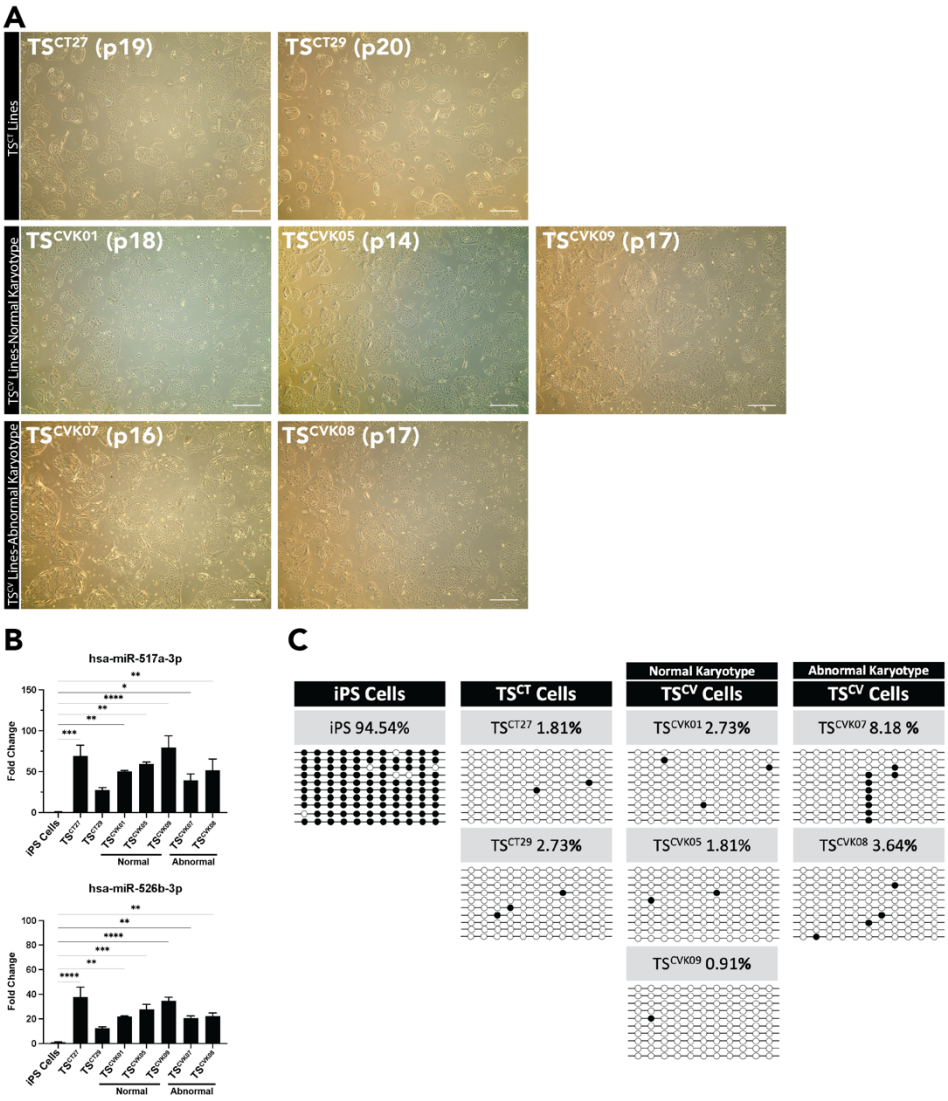

Fig. 2 Characterization of TS^{CV} cells. A) Stem state phase contrast images of the five CVS-derived TS cell lines (TS^{CVK01}, TS^{CVK05}, TS^{CVK07}, TS^{CVK08}, TS^{CVK09}) alongside images of the reference cytotrophoblast-derived TS cell lines (TS^{CT27} and TS^{CT29}) at different passage numbers (14-20). Scale bars represent 500 µm. **B)** Bar graphs depicting expression of two microRNAs (**miR**) from the C19MC cluster (hsa-miR-517a-3p and hsa-miR-526b-3p) in TS^{CT} and TS^{CV} cell lines relative to induced pluripotent stem (**iPS**) cells, measured by RT-qPCR. Data were normalized to the control miRNA, hsa-miR-103a-3p (n=3 samples per group; *p<0.05, **p<0.01, ***p<0.001, ****p<0.0001). **C)** Plots representing DNA methylation levels in the ELF5 promoter at 11 sites in TS^{CT} and TS^{CV} cell lines compared to iPS cells. Methylated sites (black) and unmethylated sites (white) are shown for 10 replicates and the average percent methylation is listed.

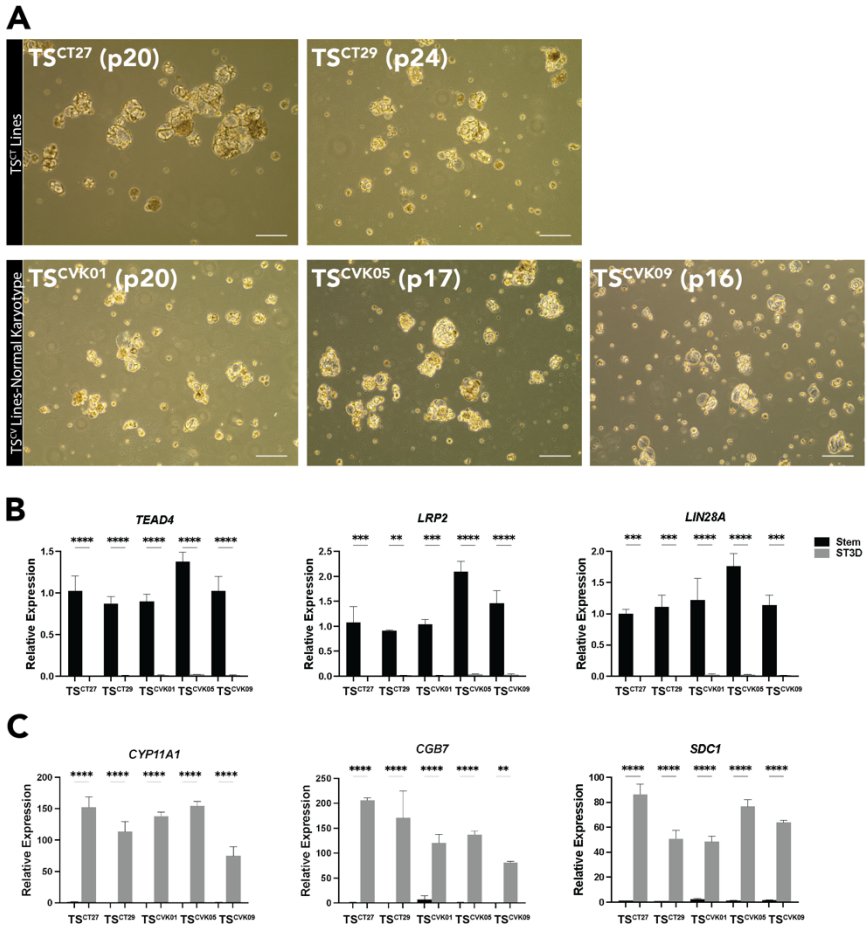

Fig. 3 TS^{CV} cell line differentiation into STB. A) Representative phase contrast images of cytotrophoblast-derived TS^{CT27} and TS^{CT29} cells and three CVS-derived TS cell lines possessing a normal karyotype, TS^{CVK01}, TS^{CVK05}, and TS^{CVK09}, cultured under STB differentiation conditions. Scale bars represent 250 µm. **B-C)** Stem cell-specific transcripts (**B;** *TEAD4*, *LRP2*, and *LIN28A*) and STB cell-specific transcripts (**C**; *CYP11A1, CGB7,* and *SDC1*) were quantified by RT-qPCR in stem (black) and STB differentiated (gray) TS^{CT27}, TS^{CT29}, TS^{CVK01}, TS^{CVK05}, and TS^{CVK09} cells (n=3 samples per group; **p<0.01, ***p<0.001, ****p<0.0001).

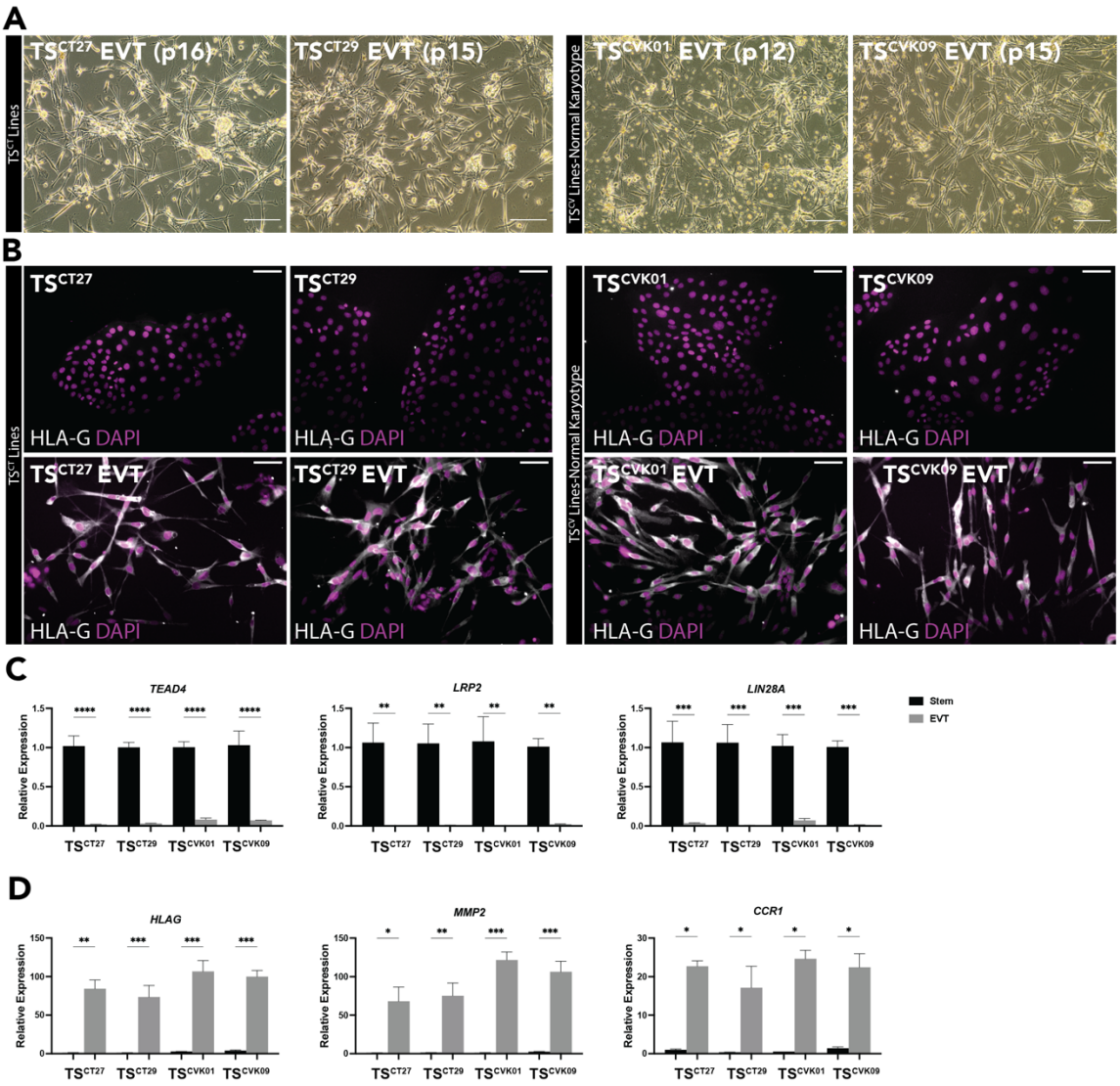

509 **Fig. 4 TS^{CV} cell line differentiation into EVT cells. A)** Representative phase contrast images of
510 cytotrophoblast-derived TS^{CT27} and TS^{CT29} cells and two CVS-derived TS cell lines possessing a normal
511 karyotype, TS^{CVK01} and TS^{CVK09}, cells cultured under EVT cell differentiation conditions. Scale bars
512 represent 250 µm **B)** Immunofluorescence detection of HLA-G (gray) by immunocytochemistry in TS^{CT}
513 and TS^{CV} cells cultured in the stem state and on day 8 of EVT cell differentiation. DAPI (magenta) stains
514 cell nuclei. Scale bars represent 100 µm. **C-D)** Stem cell-specific transcripts (**C;** *TEAD4*, *LRP2*, and
515 *LIN28A*) and EVT cell-specific transcripts (**D**; *HLA-G*, *MMP2*, and *CCR1*) were quantified by RT-qPCR in
516 stem (black) and EVT differentiated (gray) TS^{CT27}, TS^{CT29}, TS^{CVK01} and TS^{CVK09} cells (n=3 samples per
517 group; *p<0.05, **p<0.01, ***p<0.001, ****p<0.0001).
518

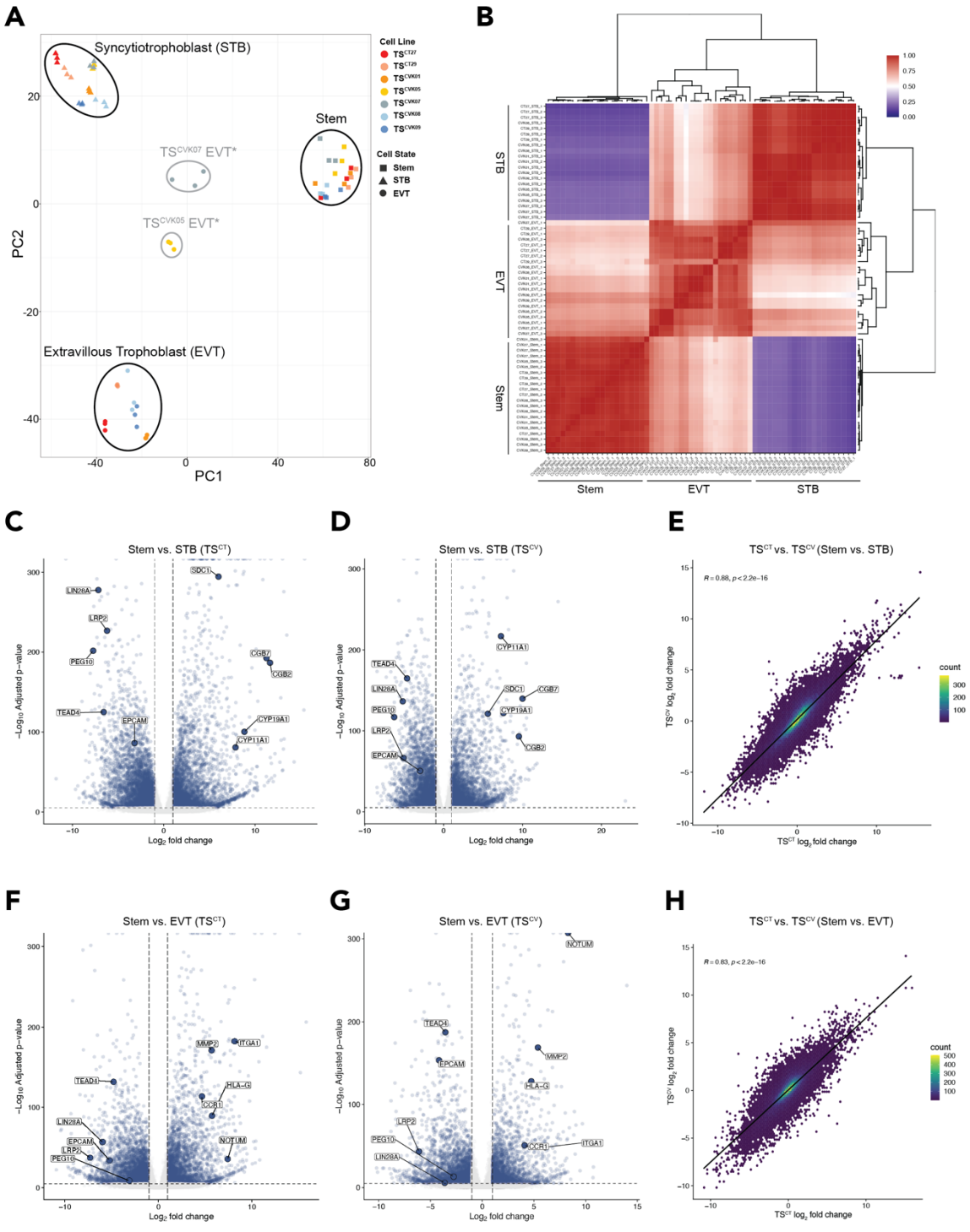

519

520 **Fig. 5 TS^{CV} and TS^{CT} cells cluster by cell state and share similar transcriptomes. A)** Principal

521 component analysis based on RNA-seq datasets generated from TS^{CT} and TS^{CV} cells cultured in the stem

522 state or following differentiation into STB and EVT cell lineages. **B)** Heat map of Pearson correlation

523 coefficients from expression profiles of stem state, STB, and EVT cell lines, with the dendrogram

generated by hierarchical clustering. **C-D)** Volcano plots depicting significantly up- and down-regulated genes based on transcripts measured by RNA-seq in stem versus STB state TS^{CT} (**C**) and TS^{CV} (**D**) cells. Gene transcript levels unchanged between stem and STB state cells are depicted in green (n=3 per group; absolute log2fold change >1, adjusted p<0.05). **E)** Two-dimensional density plot comparing gene expression changes between stem and EVT cell states in TS^{CT} (TS^{CT27} and TS^{CT29}) cells versus TS^{CV} (TS^{CVK01}, TS^{CVK05}, and TS^{CVK09}) cells (Pearson correlation coefficient (R)=0.88, p<2.2e-16). **F-G)** Volcano plots depicting significantly up- and down-regulated genes based on transcripts measured by RNA-seq in stem versus EVT states of TS^{CT} (**F**) and TS^{CV} (**G**) cells. Gene transcript levels unchanged between stem and EVT state cells are depicted in green (n=3 per group; absolute log2fold change >1, adjusted p<0.05). **H)** Two-dimensional density plot comparing gene expression changes between stem and EVT cell states in TS^{CT} (TS^{CT27} and TS^{CT29}) cells versus TS^{CV} (TS^{CVK01} and TS^{CVK09}) cells (Pearson correlation coefficient (R)=0.83, p<2.2e-16).

Table 1. CVS Specimen Data. Descriptive information for ten independent chorionic villus tissue collections (K01-K10) that were cultured for TS cell derivation. TS^{CV} cell lines were successfully established from five of the chorionic villus tissue specimens (2 XX and 3 XY cell lines). Karyotypic analysis was performed at the time of CVS collection and in TS^{CV} cell lines (after passage 10). Pregnancy outcomes are presented for each CVS tissue collection as well as select associated maternal and paternal demographics.

Video 1. Stem state and EVT-differentiated TS^{CT27} cell growth and motility. Phase contrast images were acquired every 10 min for 53 h of TS^{CT27} cells cultured under stem state or EVT cell-differentiation conditions (EVT cell differentiation protocol days 4-6).

Video 2. Stem state and EVT cell differentiated TS^{CVK01} cell growth and motility. Phase contrast images were acquired every 10 min for 53 h of TS^{CVK01} cells cultured under stem state or EVT cell differentiation conditions (EVT cell differentiation protocol days 4-6).

Video 3. Stem state and EVT cell differentiated TS^{CVK09} cell growth and motility. Phase contrast images were acquired every 10 min for 53 h of TS^{CVK09} cells cultured under stem state or EVT cell differentiation conditions (EVT cell differentiation protocol days 4-6).

References

Adusumalli J, Han CS, Beckham S, Bartholomew ML, Williams J. 2007. Chorionic villus sampling and risk for hypertensive disorders of pregnancy. *Am J Obstet Gynecol* **196**:591.e1–7; discussion 591.e7. doi:10.1016/j.ajog.2007.03.015

Aplin JD, Jones CJP. 2021. Cell dynamics in human villous trophoblast. *Hum Reprod Update* **27**:904–922. doi:10.1093/humupd/dmab015

Asanoma K, Rumi MAK, Kent LN, Chakraborty D, Renaud SJ, Wake N, Lee D-S, Kubota K, Soares MJ. 2011. FGF4-dependent stem cells derived from rat blastocysts differentiate along the trophoblast lineage. *Dev Biol* **351**:110–119. doi:10.1016/j.ydbio.2010.12.038

Bhattacharya B, Home P, Ganguly A, Ray S, Ghosh A, Islam MR, French V, Marsh C, Gunewardena S, Okae H, Arima T, Paul S. 2020. Atypical protein kinase C iota (PKCλ/ι) ensures mammalian development by establishing the maternal-fetal exchange interface. *Proc Natl Acad Sci U S A* **117**:14280–14291. doi:10.1073/pnas.1920201117

Castel G, Meistermann D, Bretin B, Firmin J, Blin J, Loubersac S, Bruneau A, Chevolleau S, Kilens S, Chariau C, Gaignerie A, Francheteau Q, Kagawa H, Charpentier E, Flippe L, François-Campion V, Haider S, Dietrich B, Knöfler M, Arima T, Bourdon J, Rivron N, Masson D, Fournier T, Okae H, Fréour T, David L. 2020. Induction of human trophoblast stem cells from somatic cells and pluripotent stem cells. *Cell Rep* **33**:108419. doi:10.1016/j.celrep.2020.108419

Cinkornpumin JK, Kwon SY, Guo Y, Hossain I, Sirois J, Russett CS, Tseng H-W, Okae H, Arima T, Duchaine TF, Liu W, Pastor WA. 2020. Naive human embryonic stem cells can give rise to cells with a trophoblast-like transcriptome and methylome. *Stem Cell Reports* **15**:198–213. doi:10.1016/j.stemcr.2020.06.003

Coorens THH, Oliver TRW, Sanghvi R, Sovio U, Cook E, Vento-Tormo R, Haniffa M, Young MD, Rahbari R, Sebire N, Campbell PJ, Charnock-Jones DS, Smith GCS, Behjati S. 2021. Inherent mosaicism and extensive mutation of human placentas. *Nature* **592**:80–85. doi:10.1038/s41586-021-03345-1

Dong C, Beltcheva M, Gontarz P, Zhang B, Popli P, Fischer LA, Khan SA, Park K-M, Yoon E-J, Xing X, Kommagani R, Wang T, Solnica-Krezel L, Theunissen TW. 2020. Derivation of trophoblast stem cells from naïve human pluripotent stem cells. *Elife* **9**:e52504. doi:10.7554/eLife.52504

Dong L, Falk RE, Williams J, Kohan M, Schreck RR. 2003. Tetrasomy 12p--unusual presentation in CVS. *Prenat Diagn* **23**:101–103. doi:10.1002/pd.538

Flowers AE, Gonzalez TL, Joshi NV, Eisman LE, Clark EL, Buttle RA, Sauro E, DiPentino R, Lin Y, Wu D, Wang Y, Santiskulvong C, Tang J, Lee B, Sun T, Chan JL, Wang ET, Jefferies C, Lawrenson K, Zhu Y, Afshar Y, Tseng H-R, Williams J, Pisarska MD. 2021. Sex differences in microRNA expression in first and third trimester human placenta†. *Biol Reprod* ioab221. doi:10.1093/biolre/ioab221

Gonzalez TL, Eisman LE, Joshi NV, Flowers AE, Wu D, Wang Y, Santiskulvong C, Tang J, Buttle RA, Sauro E, Clark EL, DiPentino R, Jefferies CA, Chan JL, Lin Y, Zhu Y, Afshar Y, Tseng H-R, Taylor K, Williams J, Pisarska MD. 2021. High-throughput miRNA sequencing of the human placenta: expression throughout gestation. *Epigenomics* **13**:995–1012. doi:10.2217/epi-2021-0055

Grigor'eva EV, Shevchenko AI, Mazurok NA, Elisaphenko EA, Zhelezova AI, Shilov AG, Dyban PA, Dyban AP, Noniashvili EM, Slobodyanyuk SYa, Nesterova TB, Brockdorff N, Zakian SM. 2009. FGF4 Independent Derivation of Trophoblast Stem Cells from the Common Vole. *PLoS ONE* **4**:e7161. doi:10.1371/journal.pone.0007161

Guo G, Stirparo GG, Strawbridge SE, Spindlow D, Yang J, Clarke J, Dattani A, Yanagida A, Li MA, Myers S, Özel BN, Nichols J, Smith A. 2021. Human naive epiblast cells possess unrestricted lineage potential. *Cell Stem Cell* **28**:1040-1056.e6. doi:10.1016/j.stem.2021.02.025

Hada M, Miura H, Tanigawa A, Matoba S, Inoue K, Ogonuki N, Hirose M, Watanabe N, Nakato R, Fujiki K, Hasegawa A, Sakashita A, Okae H, Miura K, Shikata D, Arima T, Shirahige K, Hiratani I, Ogura A. 2022. Highly rigid H3.1/H3.2-H3K9me3 domains set a barrier for cell

fate reprogramming in trophoblast stem cells. *Genes Dev* **36**:84–102. doi:10.1101/gad.348782.121

Haider S, Lackner AI, Dietrich B, Kunihs V, Haslinger P, Meinhardt G, Maxian T, Saleh L, Fiala C, Pollheimer J, Latos PA, Knöfler M. 2022. Transforming growth factor-β signaling governs the differentiation program of extravillous trophoblasts in the developing human placenta. *Proc Natl Acad Sci U S A* **119**:e2120667119. doi:10.1073/pnas.2120667119

Hanna JH, Saha K, Jaenisch R. 2010. Pluripotency and cellular reprogramming: facts, hypotheses, unresolved issues. *Cell* **143**:508–525. doi:10.1016/j.cell.2010.10.008

Hemberger M, Hanna CW, Dean W. 2020. Mechanisms of early placental development in mouse and humans. *Nat Rev Genet* **21**:27–43. doi:10.1038/s41576-019-0169-4

Hornbachner R, Lackner A, Papuchova H, Haider S, Knöfler M, Mechtler K, Latos PA. 2021. MSX2 safeguards syncytiotrophoblast fate of human trophoblast stem cells. *Proc Natl Acad Sci U S A* **118**:e2105130118. doi:10.1073/pnas.2105130118

Huang A, Adusumalli J, Patel S, Liem J, Williams J, Pisarska MD. 2009. Prevalence of chromosomal mosaicism in pregnancies from couples with infertility. *Fertil Steril* **91**:2355–2360. doi:10.1016/j.fertnstert.2008.03.044

International Standing Committee on Human Cytogenetic Nomenclature, Shaffer LG, Slovak ML, Campbell LJ, editors. 2009. ISCN 2009: an international system for human cytogenetic nomenclature (2009). Basel ; Unionville, CT: Karger.

Io S, Kabata M, Iemura Y, Semi K, Morone N, Minagawa A, Wang B, Okamoto I, Nakamura T, Kojima Y, Iwatani C, Tsuchiya H, Kaswandy B, Kondoh E, Kaneko S, Woltjen K, Saitou M, Yamamoto T, Mandai M, Takashima Y. 2021. Capturing human trophoblast development with naive pluripotent stem cells in vitro. *Cell Stem Cell* **28**:1023-1039.e13. doi:10.1016/j.stem.2021.03.013

Ishiuchi T, Ohishi H, Sato T, Kamimura S, Yorino M, Abe S, Suzuki A, Wakayama T, Suyama M, Sasaki H. 2019. Zfp281 shapes the transcriptome of trophoblast stem cells and Is essential for placental development. *Cell Reports* **27**:1742-1754.e6. doi:10.1016/j.celrep.2019.04.028

Jaju Bhattad G, Jeyarajah MJ, McGill MG, Dumeaux V, Okae H, Arima T, Lajoie P, Bérubé NG, Renaud SJ. 2020. Histone deacetylase 1 and 2 drive differentiation and fusion of progenitor cells in human placental trophoblasts. *Cell Death Dis* **11**:311. doi:10.1038/s41419-020-2500-6

Jang YJ, Kim M, Lee B-K, Kim J. 2022. Induction of human trophoblast stem-like cells from primed pluripotent stem cells. *Proc Natl Acad Sci U S A* **119**:e2115709119. doi:10.1073/pnas.2115709119

Knöfler M, Haider S, Saleh L, Pollheimer J, Gamage TKJB, James J. 2019. Human placenta and trophoblast development: key molecular mechanisms and model systems. *Cell Mol Life Sci* **76**:3479–3496. doi:10.1007/s00018-019-03104-6

Kong X, Chen X, Ou S, Wang W, Li R. 2022. Derivation of human triploid trophoblast stem cells. *J Assist Reprod Genet* **39**:1183–1193. doi:10.1007/s10815-022-02436-w

Kunath T, Yamanaka Y, Detmar J, MacPhee D, Caniggia I, Rossant J, Jurisicova A. 2014. Developmental differences in the expression of FGF receptors between human and mouse embryos. *Placenta* **35**:1079–1088. doi:10.1016/j.placenta.2014.09.008

Latos PA, Hemberger M. 2016. From the stem of the placental tree: trophoblast stem cells and their progeny. *Development* **143**:3650–3660. doi:10.1242/dev.133462

Lee B-K, Jang YJ, Kim M, LeBlanc L, Rhee C, Lee J, Beck S, Shen W, Kim J. 2019. Super-enhancer-guided mapping of regulatory networks controlling mouse trophoblast stem cells. *Nat Commun* **10**:4749. doi:10.1038/s41467-019-12720-6

Lee CQE, Gardner L, Turco M, Zhao N, Murray MJ, Coleman N, Rossant J, Hemberger M, Moffett A. 2016. What is trophoblast? A combination of criteria define human first-trimester trophoblast. *Stem Cell Reports* **6**:257–272. doi:10.1016/j.stemcr.2016.01.006

Liu X, Ouyang JF, Rossello FJ, Tan JP, Davidson KC, Valdes DS, Schröder J, Sun YBY, Chen J, Knaupp AS, Sun G, Chy HS, Huang Z, Pflueger J, Firas J, Tano V, Buckberry S, Paynter JM, Larcombe MR, Poppe D, Choo XY, O'Brien CM, Pastor WA, Chen D, Leichter AL, Naeem H, Tripathi P, Das PP, Grubman A, Powell DR, Laslett AL, David L, Nilsson SK, Clark AT, Lister R, Nefzger CM, Martelotto LG, Rackham OJL, Polo JM. 2020.

Reprogramming roadmap reveals route to human induced trophoblast stem cells. *Nature* **586**:101–107. doi:10.1038/s41586-020-2734-6

McIntosh N, Rubin C, Wang B, Williams J. 1993. Transcervical CVS sample size: correlation with placental location, cytogenetic findings, and pregnancy outcome. *Prenat Diagn* **13**:1031–1036. doi:10.1002/pd.1970131105

Muto M, Chakraborty D, Varberg KM, Moreno-Irusta A, Iqbal K, Scott RL, McNally RP, Choudhury RH, Aplin JD, Okae H, Arima T, Matsumoto S, Ema M, Mast AE, Grundberg E, Soares MJ. 2021. Intersection of regulatory pathways controlling hemostasis and hemochorial placentation. *Proc Natl Acad Sci U S A* **118**:e2111267118. doi:10.1073/pnas.2111267118

Okae H, Toh H, Sato T, Hiura H, Takahashi S, Shirane K, Kabayama Y, Suyama M, Sasaki H, Arima T. 2018. Derivation of human trophoblast stem cells. *Cell Stem Cell* **22**:50-63.e6. doi:10.1016/j.stem.2017.11.004

Papp B, Plath K. 2013. Epigenetics of reprogramming to induced pluripotency. *Cell* **152**:1324–1343. doi:10.1016/j.cell.2013.02.043

Perez-Garcia V, Lea G, Lopez-Jimenez P, Okkenhaug H, Burton GJ, Moffett A, Turco MY, Hemberger M. 2021. BAP1/ASXL complex modulation regulates epithelial-mesenchymal transition during trophoblast differentiation and invasion. *Elife* **10**:e63254. doi:10.7554/eLife.63254

Pisarska MD, Akhlaghpour M, Lee B, Barlow GM, Xu N, Wang ET, Mackey AJ, Farber CR, Rich SS, Rotter JI, Chen YI, Goodarzi MO, Guller S, Williams J. 2016. Optimization of techniques for multiple platform testing in small, precious samples such as human chorionic villus sampling. *Prenat Diagn* **36**:1061–1070. doi:10.1002/pd.4936

Ringler GE, Strauss JF. 1990. In vitro systems for the study of human placental endocrine function. *Endocr Rev* **11**:105–123. doi:10.1210/edrv-11-1-105

Robinson WP, Del Gobbo GF. 2021. Mistakes Are Common; Should We Worry about Them? *Trends Mol Med* **27**:721–722. doi:10.1016/j.molmed.2021.04.008

Ruane PT, Garner T, Parsons L, Babbington PA, Wangsaputra I, Kimber SJ, Stevens A, Westwood M, Brison DR, Aplin JD. 2022. Trophectoderm differentiation to invasive syncytiotrophoblast is promoted by endometrial epithelial cells during human embryo implantation. *Hum Reprod* **37**:777–792. doi:10.1093/humrep/deac008

Rubin CH, Williams J, Wang BB. 1993. Discrepancy in mosaic findings between chorionic villi and amniocytes: a diagnostic dilemma involving 45,X, 46,XY, and 47,XYY cell lines. *Am J Med Genet* **46**:457–459. doi:10.1002/ajmg.1320460424

Saha B, Ganguly A, Home P, Bhattacharya B, Ray S, Ghosh A, Rumi MAK, Marsh C, French VA, Gunewardena S, Paul S. 2020. TEAD4 ensures postimplantation development by promoting trophoblast self-renewal: An implication in early human pregnancy loss. *Proc Natl Acad Sci U S A* **117**:17864–17875. doi:10.1073/pnas.2002449117

Schaffers OJM, Dupont C, Bindels EM, Van Opstal D, Dekkers DHW, Demmers JAA, Gribnau J, Rijn BB van. 2022. Single-Cell Atlas of Patient-Derived Trophoblast Organoids in Ongoing Pregnancies. *Organoids* **1**:106–115. doi:https://doi.org/10.3390/organoids1020009

Shahbazi MN, Wang T, Tao X, Weatherbee BAT, Sun L, Zhan Y, Keller L, Smith GD, Pellicer A, Scott RT, Seli E, Zernicka-Goetz M. 2020. Developmental potential of aneuploid human embryos cultured beyond implantation. *Nat Commun* **11**:3987. doi:10.1038/s41467-020-17764-7

Shannon MJ, Baltayeva J, Castellana B, Wächter J, McNeill GL, Yoon JS, Treissman J, Le HT, Lavoie PM, Beristain AG. 2022. Cell trajectory modeling identifies a primitive trophoblast state defined by BCAM enrichment. *Development* **149**:dev199840. doi:10.1242/dev.199840

Sheridan MA, Zhao X, Fernando RC, Gardner L, Perez-Garcia V, Li Q, Marsh SGE, Hamilton R, Moffett A, Turco MY. 2021. Characterization of primary models of human trophoblast. *Development* **148**:dev199749. doi:10.1242/dev.199749

Shibata S, Kobayashi EH, Kobayashi N, Oike A, Okae H, Arima T. 2020. Unique features and emerging in vitro models of human placental development. *Reprod Med Biol* **19**:301–313. doi:10.1002/rmb2.12347

Soares MJ, Varberg KM, Iqbal K. 2018. Hemochorial placentation: development, function, and adaptations†. *Biology of Reproduction* **99**:196–211. doi:10.1093/biolre/ioy049

Soncin F, Morey R, Bui T, Requena DF, Cheung VC, Kallol S, Kittle R, Jackson MG, Farah O, Dumdie J, Meads M, Pizzo D, Horii M, Fisch KM, Parast MM. 2022. Derivation of functional trophoblast stem cells from primed human pluripotent stem cells. *Stem Cell Reports* **17**:1303–1317. doi:10.1016/j.stemcr.2022.04.013

Stranc LC, Evans JA, Hamerton JL. 1997. Chorionic villus sampling and amniocentesis for prenatal diagnosis. *Lancet* **349**:711–714. doi:10.1016/S0140-6736(96)08169-X

Sun T, Gonzalez TL, Deng N, DiPentino R, Clark EL, Lee B, Tang J, Wang Y, Stripp BR, Yao C, Tseng H-R, Karumanchi SA, Koeppel AF, Turner SD, Farber CR, Rich SS, Wang ET, Williams J, Pisarska MD. 2020. Sexually Dimorphic Crosstalk at the Maternal-Fetal Interface. *J Clin Endocrinol Metab* **105**:dgaa503. doi:10.1210/clinem/dgaa503

Takahashi S, Okae H, Kobayashi N, Kitamura A, Kumada K, Yaegashi N, Arima T. 2019. Loss of p57KIP2 expression confers resistance to contact inhibition in human androgenetic trophoblast stem cells. *Proc Natl Acad Sci U S A*. doi:10.1073/pnas.1916019116

Tanaka S, Kunath T, Hadjantonakis AK, Nagy A, Rossant J. 1998. Promotion of trophoblast stem cell proliferation by FGF4. *Science* **282**:2072–2075.

Varberg KM, Iqbal K, Muto M, Simon ME, Scott RL, Kozai K, Choudhury RH, Aplin JD, Biswell R, Gibson M, Okae H, Arima T, Vivian JL, Grundberg E, Soares MJ. 2021. ASCL2 reciprocally controls key trophoblast lineage decisions during hemochorial placenta development. *Proc Natl Acad Sci U S A* **118**. doi:10.1073/pnas.2016517118

Viukov S, Shani T, Bayerl J, Aguilera-Castrejon A, Oldak B, Sheban D, Tarazi S, Stelzer Y, Hanna JH, Novershtern N. 2022. Human primed and naïve PSCs are both able to differentiate into trophoblast stem cells. *Stem Cell Reports* S2213-6711(22)00457-X. doi:10.1016/j.stemcr.2022.09.008

Wang BB, Rubin CH, Williams J. 1993. Mosaicism in chorionic villus sampling: an analysis of incidence and chromosomes involved in 2612 consecutive cases. *Prenat Diagn* **13**:179–190. doi:10.1002/pd.1970130305

Wang BT, Peng W, Cheng KT, Chiu SF, Ho W, Khan Y, Wittman M, Williams J. 1994. Chorionic villi sampling: laboratory experience with 4,000 consecutive cases. *Am J Med Genet* **53**:307–316. doi:10.1002/ajmg.1320530402

Wang L-J, Chen C-P, Lee Y-S, Ng P-S, Chang G-D, Pao Y-H, Lo H-F, Peng C-H, Cheong M-L, Chen H. 2022. Functional antagonism between ΔNp63α and GCM1 regulates human trophoblast stemness and differentiation. *Nat Commun* **13**:1626. doi:10.1038/s41467-022-29312-6

Wei Y, Wang T, Ma L, Zhang Y, Zhao Y, Lye K, Xiao L, Chen C, Wang Z, Ma Y, Zhou X, Sun F, Li W, Dunk C, Li S, Nagy A, Yu Y, Pan G, Lye SJ, Shan Y. 2021. Efficient derivation of human trophoblast stem cells from primed pluripotent stem cells. *Sci Adv* **7**:eabf4416. doi:10.1126/sciadv.abf4416

Williams J, Medearis AL, Bear MB, Kaback MM. 1987. Chorionic villus sampling is associated with normal fetal growth. *Am J Obstet Gynecol* **157**:708–712. doi:10.1016/s0002-9378(87)80034-0

Williams J, Wang BB, Rubin CH, Aiken-Hunting D. 1992. Chorionic villus sampling: experience with 3016 cases performed by a single operator. *Obstet Gynecol* **80**:1023–1029.

Yanagida A, Spindlow D, Nichols J, Dattani A, Smith A, Guo G. 2021. Naive stem cell blastocyst model captures human embryo lineage segregation. *Cell Stem Cell* **28**:1016-1022.e4. doi:10.1016/j.stem.2021.04.031

Yuen RKC, Robinson WP. 2011. Review: A high capacity of the human placenta for genetic and epigenetic variation: implications for assessing pregnancy outcome. *Placenta* **32 Suppl 2**:S136-141. doi:10.1016/j.placenta.2011.01.003